



Deposited via The University of Leeds.

White Rose Research Online URL for this paper:

<https://eprints.whiterose.ac.uk/id/eprint/176062/>

Version: Accepted Version

Proceedings Paper:

Wang, C, Sivan, M, Bao, T et al. (2021) 3D Free Reaching Movement Prediction of Upper-limb Based on Deep Neural Networks. In: 2021 10th International IEEE/EMBS Conference on Neural Engineering (NER). 2021 10th International IEEE/EMBS Conference on Neural Engineering (NER), 04-06 May 2021, Online. IEEE. ISBN: 978-1-7281-4338-5. ISSN: 1948-3554. EISSN: 1948-3554.

<https://doi.org/10.1109/ner49283.2021.9441350>

Reuse

Items deposited in White Rose Research Online are protected by copyright, with all rights reserved unless indicated otherwise. They may be downloaded and/or printed for private study, or other acts as permitted by national copyright laws. The publisher or other rights holders may allow further reproduction and re-use of the full text version. This is indicated by the licence information on the White Rose Research Online record for the item.

Takedown

If you consider content in White Rose Research Online to be in breach of UK law, please notify us by emailing eprints@whiterose.ac.uk including the URL of the record and the reason for the withdrawal request.

3D Free Reaching Movement Prediction of Upper-limb Based on Deep Neural Networks

Chao Wang, Manoj Sivan, Tianzhe Bao, Guqiang Li, Shengquan Xie

Abstract—Quantitative assessment of motor disorder is one of the main challenges in the field of stroke rehabilitation. This paper proposes a simplified kinematic model for human upper limb(UL) using seven main joints of both the dominant and non-dominant side. With this model, a deep neural network (DNN) is used to predict the 3D free reaching movement of UL of a healthy participant. The experimental results show that the prediction trajectories can achieve high similarities with trajectories of real movements, indicating the promising accuracy in 3D movement estimation of UL achieved by the DNN. With the capability of identifying specific reaching movements in real-time, the trajectories predicted by this data-driven model can be utilized to inform the rehabilitation assessment and training in the future studies as a personalized therapy approach.

Keywords: 3D, upper limb, rehabilitation assessment, data-driven, movement prediction

I. INTRODUCTION

Stroke is the leading cause of adult-onset disability in the world [1]. With an increasing number of patients suffering stroke, a more reliable approach for rehabilitation assessment and training is required [2]. Motor function assessment plays a significant role in rehabilitation as it directly illustrates the effectiveness of rehabilitation therapy [3], [4]. To provide a reliable assessment of motor function, motor control and the trajectory planning strategies of the central nervous system (CNS) need to be understood [5]. Reaching is one of the simplest movements in daily life. It has been frequently used in the motor function assessment for patients with motor disorder [6]–[9]. A better understanding of normal reaching movement could improve the motor function assessment. More specifically, accurately modeling of reaching pattern is the key point to quantitatively measure the difference between healthy individuals and those with arm impairment.

Previous literature has verified that CNS does not randomly control the limbs and plan the movement during the reaching [7], [8], [10]. Among the infinite number of trajectories that can be chosen due to the redundancy of the UL motor system [7], [8], [10], [11], it is considered that the CNS tries to minimize the movement-related costs in the control of UL movement [12]. Therefore, the unconstrained reaching movement trajectories of with natural speed would be repetitive in the same reaching task [13], [14]. In other words, there is an optimal trajectory selected by the CNS when a person is doing a specific motor task. Although which strategies exactly employed are still largely unclear, it is possible to model the reaching process and predict the movement, which would prove useful in the rehabilitation assessment and training.

Earlier studies reported kinematic and dynamic models which aim to discover these control strategies behind the

reaching movement. The vast majority of these models are developed to generate the prediction trajectory by optimizing a criterion function. Flash and Hogan proposed their minimum-jerk model which aimed to optimize the rate of acceleration changes of hand [15]. Hasan reported a model minimizing the effort of joints [16]. Todorov presented a new approach which aimed to minimize the reaching error and energy cost together [17]. Pham reported a minimum acceleration model for goal-oriented locomotion which was adapted from the smoothness maximization models [18]. Dongsung and Terrener presented a power law [19] and smoothness maximization model to generate the target trajectory [20]. DeWolf presented a spiking neuron model to simulate the planar arm movement [21]. Dounskaia proposed a cost function which represents the neural effort for joint coordination [22]. Although these models improved the understanding of the potential laws employed by the CNS, it is still hard to identify the complex motor system of UL, leading to the lack of accurate prediction results from these kinematic and dynamic models to inform the rehabilitation assessment. Additionally, 3D movement prediction of upper-limb multi-joint still needs to be studied.

Deep learning (DL) techniques have been widely applied to various fields due to their incredible capability in complex system identification. Many recent studies have employed the DL approaches to develop the models that predict the trajectory of UL reaching movement. Bernabucci presented a bio-inspired artificial neural networks (ANN) model to predict upper human arm planar motion [23]. Genc reported a new convolutional neural network (CNN) structure to overcome the scalability and robustness difficulties in complex system identification [24]. Gilra proposed a non-linear dynamics prediction model by using recurrent spiking neural networks [25]. Tieck trained the liquid state machine (LSM) with reinforcement learning (RL) to learn the continuous muscle control of target reaching task [26]. Lang stated a multi-layer Gaussian process (GP) model [27]. However, these models still focus on planar or 3D single-joint movement prediction, while the customized motor function assessment of stroke requires the model to predict 3D movements of the multiple joints of UL.

This paper proposes a data-driven method for the prediction of 3D movements of multiple joints of UL during reaching. Firstly, we established a simplified kinematic model and extracted seven main joints of both the dominant and non-dominant side of UL. Based on this model, a deep neural network was developed and trained with the movement data from one healthy participant. Finally, the performance of the

DNN model was analyzed for both sides.

II. METHODOLOGY

A. Simplified Skeletons Structure

Based on UL framework proposed by the International Society of Biomechanics (ISB) [28], a simplified kinematic model of human UL is defined. It contains seven segments which are the trunk, right/left upper arm, right/left forearm, right/left shoulder. These segments are connected by seven main joints of UL. Only the connection at the elbow and 8th thoracic vertebra are one degree of freedom joints, the others are three degrees of freedom joints. Fig. 1(a) shows one side of the kinematic model used in this study. It contains the main joints on this side of UL. With this kinematic model, an upper-limb marker model (a set of marker placements) is presented in Fig.1(b). There are 19 reflective markers to identify the kinematics required by the movement prediction model.

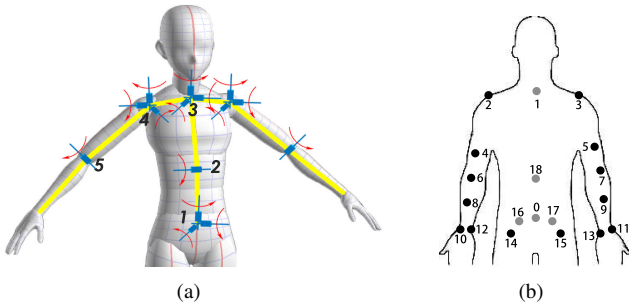


Fig. 1. (a) UL skeleton model which is composed of 5 main joints on one side (1. sacroiliac, 2. 8th thoracic vertebra, 3. 7th cervical vertebra, 4. shoulder and 5. elbow). (b) The marker model of optical tracking: 0. sacrum, 1. C7 (7th cervical vertebra), 2/3. right/left Shoulder, 4/5. right/left upper arm, 6/7. right/left elbow, 8/9. right/left forearm, 10/11. right/left wrist marker B, 12/13. right/left wrist marker A, 14/15. right/left anterior superior iliac, 16/17. right/left posterior superior iliac, 18. 8th thoracic vertebra.

B. Experiment Setup

This study was approved by the University of Leeds Ethics Committee (Reference MEEC 18-005). The data collection experiment involved one 25-year-old right hand dominant male healthy participant after providing informed consent. The participant was asked to complete 6 blocks tests for both the dominant and non-dominant side; each block contains 20 free reaching tasks with a natural speed, making a total of 120 times repetitions for each side movement. The 19 reflective markers were placed on the skin to identify the segments and joints mentioned in the kinematic model. A Universal Robot (UR) was employed to provide the targets during the reaching tasks.

As shown in Fig. 2, the participant sat on the chair with a seat-belt fastened to remain in his initial position and restrain the compensatory movement. Firstly, the participant was asked to freely move his arm in the 3-D space freely but without trunk movement and shoulder displacement to measure the range of motion of his arms. Then, a set of target positions were determined based on the range of motion.

Some of the targets' positions were set in the range of motion, and some were not.

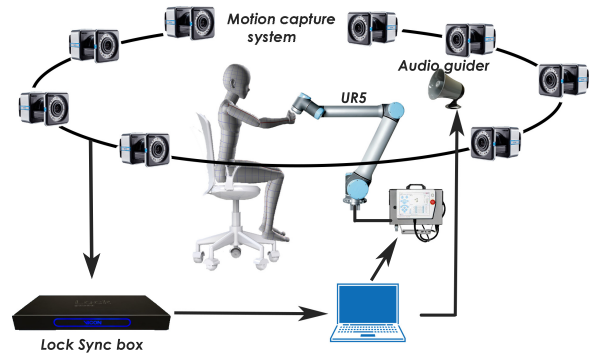


Fig. 2. Basic experimental setup of the reaching test and data collection.

At the beginning of each task, a new target position was given by UR, and an audio guider was employed to remind the participant when to start the task. After completing each task, the participant was given a short period to relax. During every task, the Vicon Motion Capture system (Vicon Motion Systems, Ltd., Oxford, England) with 8 Vero-cameras were used to record all the markers' trajectories, velocities, and also acceleration along three-axes (x, y, z) with 250 Hz sampling rate. After each block, there was a longer period for participants to rest in case the muscle fatigue may impact the participant's performance.

C. Data Pre-processing

The entire reaching procedure has two stages, the forward reaching stage and the recovery stage. Due to the scope of this study, only the first stage data was extracted and used to train our data-driven model. Thus, firstly, the velocity profile of marker 10 (for dominant side) or marker 11 (for non-dominant side) during the reaching movement was calculated. Based on this profile, the movement onset and offset instances, t_{on} and t_{off} , of this stage were determined both by 5% maximum velocity [29], [30].

In order to train the DNN to predict the movement trajectory, the raw reaching data of each side was reconstructed as a specific form. From the extracted data samples, the target position and participant's initial pose, including C7, T8, and the test-side shoulder, elbow, and hand positions of all reaching movement were also identified as the input of the DNN model. For each data sample, the input is an 18×1 feature matrix (FM). Thus, the input FMs of all data samples can be clustered into one batch and reshaped as an $18 \times 1 \times N$ matrix as the input (X) of our model, where N is the total number of data samples. Moreover, 100 frames of data were re-sampled from every forward reaching stage. Each of these frames contains the 3D coordinates of C7, T8, shoulder, elbow, and hand. Thus, the coordinates of each frame can be described as a 5×3 matrix. For the total 100 frames, a 5×300 coordinate matrix can be found. The coordinates matrix of each data sample was reshaped to be a 1500×1 matrix. As a result, we got a $1500 \times 1 \times N$ matrix as the expected outputs (Y) of our model by clustering

the coordinates matrices of all data samples, where N is the number of the sample collected from each side reaching movement. Finally, for each side movement, the input matrix X and output matrix Y of this DNN model were determined.

D. DNN Architecture

The DNN model contains 1 input layer, 1 output layer, 3 fully-connected (FC) layers, and 1 dropout layer. The input layer has 18 units to read the initial FM. The first hidden layer is fully-connected with the input layer with 256 units and ReLU activation function. After this, a dropout layer is applied to avoid the over-fitting problem. The third layer is also an FC layer but with 750 units activated by the Sigmoid activation function. Then, the last FC layer has 750 units with ReLU. Finally, an output layer is FC with the last FC layer with 1500 output units. Fig. 3 shows the architecture of this model. The DNN architecture and the hyper-parameters are determined experimentally.

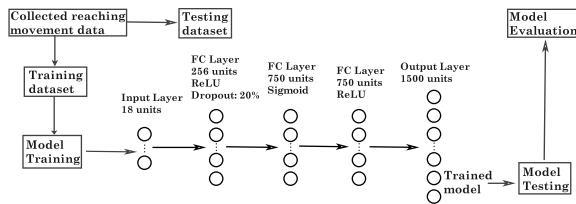


Fig. 3. The training process of the movement prediction deep neural networks.

E. Model Training

The entire dataset was split into five folds, where four of them were used for model training and one was retained for testing. To avoid over-fitting, the four folds of samples were further split as the training set (60%) and the validation set (40%). The Mean Squared Error(MSE) was employed to tune the DNN's hyper-parameters during the training process. The full batch learning strategy was applied to calculate the gradient more accurately. Then, based on such a strategy, the DNN was trained in 1000 epochs with the RMSprop optimizer whose learning rate was set as 0.001, and the dropout rate of the dropout layers was set as 0.2.

F. Model Evaluation

Due to the specific objective of this model, we evaluated the performance of the model by calculating the similarity between the prediction trajectory and the real trajectory of all joints. The similarity is measured by the Discrete Fréchet distance (coupling distance) [31] which is defined as follow:

$$\delta_F(P, Q) = \min_{\substack{\alpha: [t_s, t_e] \rightarrow [0, N] \\ \beta: [t_s, t_e] \rightarrow [0, M]}} \left\{ \max_{t \in [t_s, t_e]} d(P(\alpha(t)), Q(\beta(t))) \right\}$$

where t_s and t_e is the start and end time instance, respectively, N, M are the end position of trajectory P and Q , $P(\alpha(t))$ and $Q(\beta(t))$ are two different trajectories, $\alpha(t)$ and $\beta(t)$ are the position description function of P, Q respectively. Additionally, $\alpha(t_s) = 0, \alpha(t_e) = N, \beta(t_s) = 0, \beta(t_e) = M$. For every joint, a smaller coupling distance between the prediction and expectation means a higher similarity.

III. RESULT AND DISCUSSION

The two columns of Fig.4 show the prediction and expected trajectories of the dominant(left) and non-dominant(right) sides, respectively. The prediction results and the real trajectories show a high correlation. For the dominant side, the prediction trajectories of hand and elbow coincide the real trajectories, see Fig.4(a) and Fig.4(b). The generated trajectories of shoulder, C7 and T8 were not that well coinciding with the expected trajectories. Nevertheless, the shapes of these prediction trajectories show high similarity with the expected movement trajectories, see Fig.4(c), Fig.4(d) and Fig.4(e). This indicates that the DNN predicts the dominant side movement with promising high accuracy with the hand's coupling distance ranged from about 37 to 62 mm. For the non-dominant side movement, the prediction results are well coincident with the real trajectories, see Fig.4(f) and Fig.4(g). In contrast, the generation results of shoulder, C7 and T8 are not very close to the expected trajectories. The reason might be that the dominant side is well-trained in daily life while the non-dominant side is less used. It, however, still shows similar shapes between prediction and real trajectories for non-dominant side, see Fig.4(h), Fig.4(i) and Fig.4(j). Thus, the prediction results of the non-dominant side are still highly similar to the real movements. These results are consistent with Fig.5(a) and Fig.5(b).

The coupling distances between the prediction movements and real movements were calculated for the testing samples, see Fig.5(a) and Fig.5(b). The blue bars show the average coupling distance between the prediction and real trajectories in the testing dataset. The error bars show the standard deviation of these coupling distances. It is clear that the predictions on the dominant side are stable than the non-dominant side. The error rates of predictions of hand and elbow are lower than that of shoulder, C7 and T8 for both sides.

The average coupling distance between these predicted trajectories and expected trajectories of testing samples are calculated and compared with the average coupling distance between each pair of the trajectories on the training dataset, see Table.I and Table.II. For the dominant side, the average coupling distance of hand and elbow trajectories on the test dataset is about 60 mm and 50 mm, respectively, which is much lower than that on the training dataset. By contrast, the coupling distance of shoulder, C7 and T8 are much closer to the average coupling distance on the training dataset. It indicates that the prediction of hand and elbow is actually better than the prediction of shoulder, C7 and T8, even if the average coupling distance of the latter is slightly lower than the former. However, the average coupling distances of shoulder, C7 and T8 are still much lower than those on the training dataset. It illustrates that the prediction results of dominant side movements have high similarity with the real movement trajectories. For the non-dominant side, the significant differences between the average coupling distance on the testing and training dataset can be found for hand and

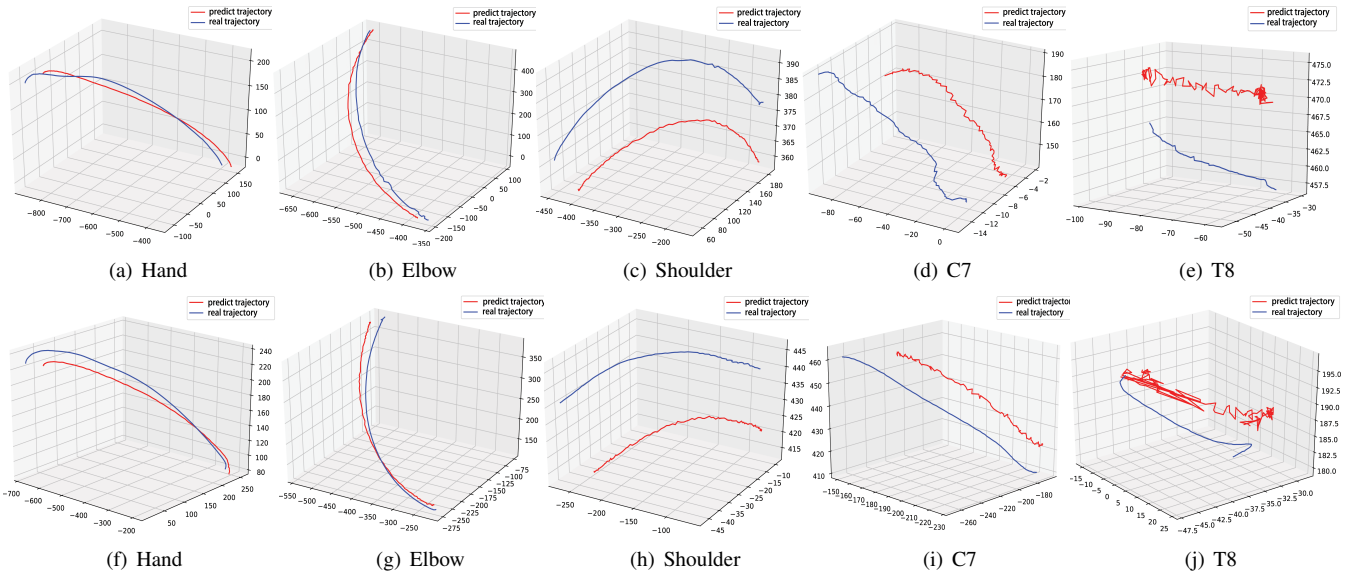


Fig. 4. The figures of the first and the second row show the prediction (in red) and expected trajectories (in blue) of the dominant side and non-dominant side, respectively.

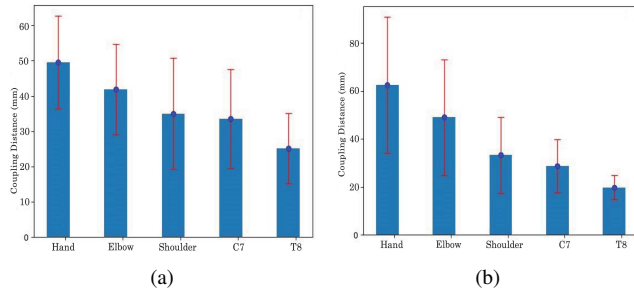


Fig. 5. (a) The average coupling distance between prediction and real trajectory of the test samples (dominant side) (b) The average coupling distance between prediction and real trajectory of the test samples (non-dominant side).

elbow. Thus, the prediction trajectories of hand and elbow are very close to the real trajectories. The average coupling distance of shoulder is much closer to the average coupling distance on the training dataset but still lower. For C7 and T8, these values are slightly higher than the average coupling distance on the training dataset. Thus, the prediction of these two joints still needs to be improved. For the non-dominant

TABLE I

The average coupling distance (Dominant side)

Joint name	Hand	Elbow	Shoulder	C7	T8
Training (mm)	299.47	248.33	178.87	139.84	88.94
Testing (mm)	62.44	49.01	33.24	28.75	19.74

side, the coupling distances between the predicted movement and expected movement are much higher than the dominant side. It means that the precision of the DNN model for the dominant side is higher than the non-dominant side. The reason might be that the target settings of the dominant side experiment are much more reasonable. As a result, the data samples collected for the dominant side could indicate the whole range of motion of the participant's UL. As shown in Table. I and Table. II, the average coupling distances for the C7, T8 of the dominant side are much higher than the

non-dominant side, indicating the diversity of the dominant movement dataset is higher than the non-dominant side. In a word, the DNN shows a better performance on the dominant side movement prediction compared to the non-dominant side, while the non-dominant side prediction results still could be improved by increasing the diversity of the dataset.

TABLE II

The average coupling distance (Non-dominant side)

Joint name	Hand	Elbow	Shoulder	C7	T8
Training (mm)	282.42	229.93	116.71	28.12	15.18
Testing (mm)	49.49	41.85	35.02	33.47	25.17

The presented model provides a good solution for the 3D free reaching movement prediction of upper-limb joints with promising accuracy. As far as we are aware, such a model of trajectory prediction for upper-limb multiple joints' 3D reaching movements has not been described before. It inspires a novel approach of motor function assessment based on which the customized assessment technique for the stroke patients could be developed. To achieve this, we plan to do further testing in a larger sample of healthy subjects to improve the generalization ability of this model.

IV. CONCLUSIONS AND FUTURE WORK

The DNN model shows potential in identifying goal-oriented reaching test's trajectory with hand's coupling distance from about 37 to 62 mm for the dominant side and 36 to 91 mm for the non-dominant side. The generated trajectories are relatively close to the real trajectories. For the dominant side, the trajectories generated by the DNN coincided well with the corresponding real trajectories, especially for the hand and elbow, where the prediction trajectories and expected trajectories were almost the same with the coupling distance shown in Table. I. The prediction results of shoulder, neck and trunk also showed high correlation (see Table. I) with the real movements. For the non-dominant side, the movement of hand and elbow generated by the DNN were

also highly representative of the participant's movement. This includes the movement of shoulder, neck, and trunk. In summary, the presented DNN model gives a good prediction (with short coupling distance, see Table. I and Table. II) of 3D reaching movements for multiple joints of human UL. In the future research, more healthy participants will be involved to validate this model further. This prediction model will also be applied to stroke survivors to estimate the deviation from the normal expected movement pattern and inform the rehabilitation assessment and training.

ACKNOWLEDGMENT

The authors would like to acknowledge the Institute of Rehabilitation Engineering, Binzhou Medical University for their support to this project.

REFERENCES

- [1] M. Naghavi, "Global, regional, and national burden of suicide mortality 1990 to 2016: systematic analysis for the Global Burden of Disease Study 2016," *British Medical Journal*, p. 194, 2019.
- [2] "Stroke: a global response is needed," WHO.int, 2016. Available: <https://www.who.int/bulletin/volumes/94/9/16-181636/en/>. [Accessed: 03- Sep- 2019].
- [3] D. Gladstone, C. Danells and S. Black, "The Fugl-Meyer Assessment of Motor Recovery after Stroke: A Critical Review of Its Measurement Properties," *Neurorehabilitation and Neural Repair*, vol. 16, no. 3, pp. 232-240, 2002.
- [4] N. Nordin, S. Xie and B. Wünsche, "Assessment of movement quality in robot- assisted upper limb rehabilitation after stroke: a review," *Journal of NeuroEngineering and Rehabilitation*, vol. 11, no. 1, p. 137, 2014.
- [5] T. Mulder, W. Zijlstra and A. Geurts, "Assessment of motor recovery and decline," *Gait & Posture*, vol. 16, no. 2, pp. 198-210, 2002.
- [6] Murphy, Willén and Sunnerhagen, "Reduced Kinematic Redundancy and Motor Equivalence During Whole-Body Reaching in Individuals With Chronic Stroke," *Neurorehabilitation and Neural Repair*, vol. 32, no. 2, pp. 175-186, 2018.
- [7] Y. Tomita, M. Rodrigues and M. Levin, "Upper Limb Coordination in Individuals With Stroke: Poorly Defined and Poorly Quantified," *Neurorehabilitation and Neural Repair*, vol. 31, no. 10-11, pp. 885-897, 2017.
- [8] Y. Tomita, A. Mullick and M. Levin, "Reduced Kinematic Redundancy and Motor Equivalence During Whole-Body Reaching in Individuals With Chronic Stroke," *Neurorehabilitation and Neural Repair*, vol. 32, no. 2, pp. 175-186, 2018.
- [9] Q. Yang, Y. Yang, J. Luo, L. Li, T. Yan and R. Song, "Kinematic Outcome Measures using Target-Reaching Arm Movement in Stroke," *Annals of Biomedical Engineering*, vol. 45, no. 12, pp. 2794-2803, 2017.
- [10] Y. Uno, M. Kawato and R. Suzuki, "Formation and control of optimal trajectory in human multijoint arm movement," *Biological Cybernetics*, vol. 61, no. 2, 1989.
- [11] L. Ting et al., "Neuromechanical Principles Underlying Movement Modularity and Their Implications for Rehabilitation," *Neuron*, vol. 86, no. 1, pp. 38-54, 2015.
- [12] R. Ranganathan, A. Adewuyi and F. Mussa-Ivaldi, "Learning to be Lazy: Exploiting Redundancy in a Novel Task to Minimize Movement-Related Effort," *Journal of Neuroscience*, vol. 33, no. 7, pp. 2754-2760, 2013.
- [13] P. Morasso, "Three dimensional arm trajectories," *Biological Cybernetics*, vol. 48, no. 3, pp. 187-194, 1983.
- [14] C. Atkeson and J. Hollerbach, "Kinematic features of unrestrained vertical arm movements," *The Journal of Neuroscience*, vol. 5, no. 9, pp. 2318-2330, 1985.
- [15] T. Flash and N. Hogan, "The coordination of arm movements: an experimentally confirmed mathematical model," *The Journal of Neuroscience*, vol. 5, no. 7, pp. 1688-1703, 1985.
- [16] Z. Hasan, "Optimized movement trajectories and joint stiffness in unperturbed, inertially loaded movements," *Biological Cybernetics*, vol. 53, no. 6, pp. 373-382, 1986.
- [17] E. Todorov and M. Jordan, "Optimal feedback control as a theory of motor coordination," *Nature Neuroscience*, vol. 5, no. 11, pp. 1226-1235, 2002.
- [18] Q. Pham, H. Hicheur, G. Arechavaleta, J. Laumond and A. Berthoz, "The formation of trajectories during goal-oriented locomotion in humans. II. A maximum smoothness model," *European Journal of Neuroscience*, vol. 26, no. 8, pp. 2391-2403, 2007.
- [19] F. Lacquaniti, C. Terzuolo and P. Viviani, "The law relating the kinematic and figural aspects of drawing movements," *Acta Psychologica*, vol. 54, no. 1-3, pp. 115-130, 1983.
- [20] D. Huh and T. Sejnowski, "Spectrum of power laws for curved hand movements," *Proceedings of the National Academy of Sciences*, vol. 112, no. 29, pp. E3950-E3958, 2015.
- [21] T. DeWolf, T. Stewart, J. Slotine and C. Eliasmith, "A spiking neural model of adaptive arm control," *Proceedings of the Royal Society B: Biological Sciences*, vol. 283, no. 1843, p. 20162134, 2016.
- [22] N. Dounskaia and Y. Shimansky, "Strategy of arm movement control is determined by minimization of neural effort for joint coordination," *Experimental Brain Research*, vol. 234, no. 6, pp. 1335-1350, 2016.
- [23] I. Bernabucci, S. Conforto, M. Schmid and T. D'Alessio, "A bio-inspired controller of an upper arm model in a perturbed environment," *2007 3rd International Conference on Intelligent Sensors, Sensor Networks and Information, 2007*.
- [24] S. Genc, "Parametric system identification using deep convolutional neural networks," in *2017 International Joint Conference on Neural Networks (IJCNN)*, 2017.
- [25] A. Gilra and W. Gerstner, "Predicting non-linear dynamics by stable local learning in a recurrent spiking neural network," *eLife*, vol. 6, 2017.
- [26] J. Tieck, M. Pogančić, J. Kaiser, A. Roennau, M. Gewaltig and R. Dillmann, "Learning Continuous Muscle Control for a Multi-joint Arm by Extending Proximal Policy Optimization with a Liquid State Machine," *Artificial Neural Networks and Machine Learning - ICANN 2018*, pp. 211-221, 2018.
- [27] M. Lang, "Human Motor Behavior Prediction through Gaussian Process Modeling on Manifolds," Ph.D., Technical University of Munich, 2019.
- [28] G. Wu et al., "ISB recommendation on definitions of joint coordinate systems of various joints for the reporting of human joint motion-Part II: shoulder, elbow, wrist and hand," *Journal of Biomechanics*, vol. 38, no. 5, pp. 981-992, 2005.
- [29] M. Johnson et al., "Bilateral assessment of functional tasks for robot-assisted therapy applications," *Medical & Biological Engineering & Computing*, vol. 49, no. 10, pp. 1157-1171, 2011.
- [30] S. Balasubramanian, R. Colombo, I. Sterpi, V. Sanguineti and E. Burdet, "Robotic Assessment of Upper Limb Motor Function After Stroke," *American Journal of Physical Medicine & Rehabilitation*, vol. 91, pp. S255-S269, 2012.
- [31] E. Chambers, É. Colin de Verdière, J. Erickson, S. Lazard, F. Lazarus and S. Thite, "Homotopic Fréchet distance between curves or, walking your dog in the woods in polynomial time," *Computational Geometry*, vol. 43, no. 3, pp. 295-311, 2010.